Title
Comparison of Methods for Determining Eigenmodes of Elliptical Waveguides

Authors
Goldberg, D.A.
Laslett, L.J.
Rimmer, R.A.

Publication Date
1990-04-01

LBL-29051
UC-410

Lawrence Berkeley Laboratory
UNIVERSITY OF CALIFORNIA

Accelerator & Fusion
Research Division

Comparison of Methods for Determining Eigenmodes of Elliptical Waveguides

D.A. Goldberg, L.J. Laslett, and R.A. Rimmer

April 1990

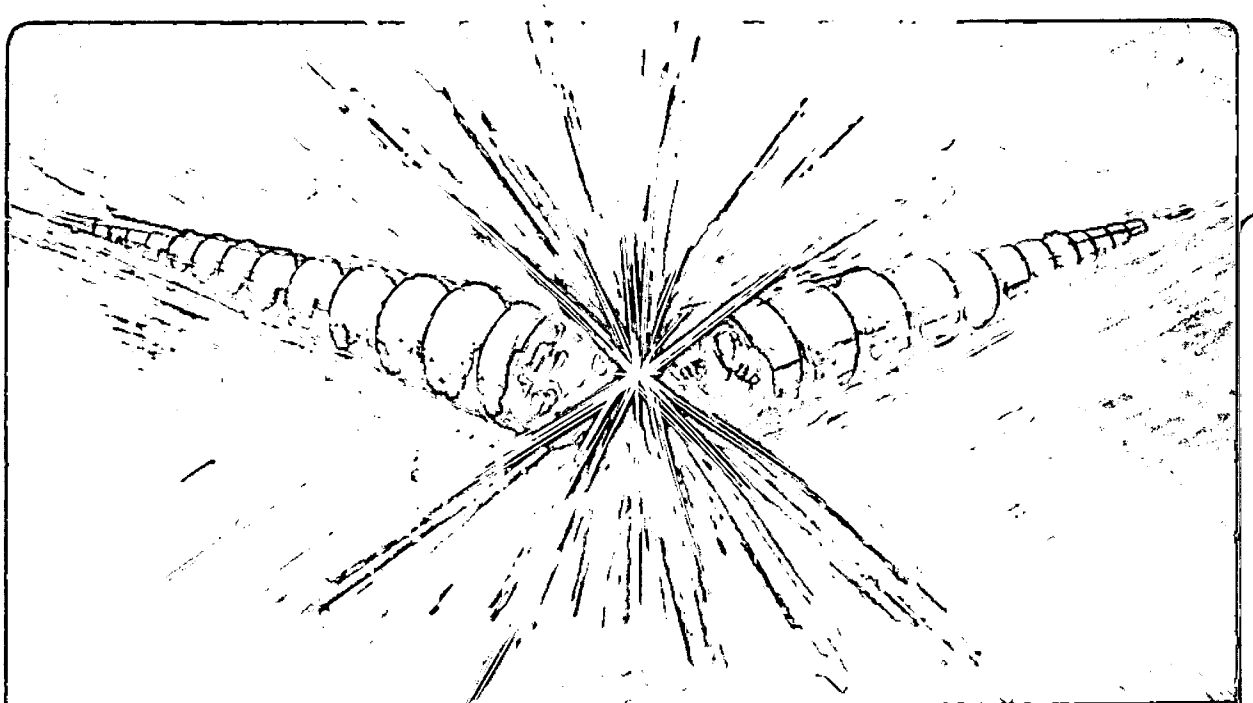

Prepared for the U.S. Department of Energy under Contract Number DE-AC03-76SF00098.

DISCLAIMER

LBL-29051

Comparison of Methods for Determining Eigenmodes of Elliptical Waveguides*

D. A. Goldberg, L. J. Laslett, and R. A. Rimmer

Accelerator and Fusion Research Division
Lawrence Berkeley Laboratory
1 Cyclotron Road
Berkeley, CA 94720

April 1990

*This work was supported by the Director, Office of Energy Research, Office of Basic Energy Sciences, Materials Sciences Division of the U.S. Department of Energy, under Contract No. DE-AC03-76SF00098

COMPARISON OF METHODS FOR DETERMINING EIGENMODES OF ELLIPTICAL WAVEGUIDES

D.A. Goldberg, L.J. Laslett, and R.A. Rimmer

1. Introduction

Waveguide modes (particularly their cutoff frequencies) in pipes of elliptical cross section are of interest in connection with impedance estimates for the Advanced Light Source (ALS). First, there will be sections where the ALS beam pipe will in fact be elliptical. Second, for those regions where the cross-section is not elliptical (e.g. the regions containing the ante-chamber), modes and their cutoff frequencies will have to be obtained using numerical field solvers such as URMEL-T; it was felt to be desirable to check the numerical accuracy of such codes by examining their results for a problem with "known" solutions, e.g., the elliptical waveguide.

Solutions to the elliptical waveguide problem have been worked out in a classic paper by L-J Chu [1], which gives field plots for the lowest few modes, as well as a graph of cutoff frequency *vs* eccentricity for those modes. Initial URMEL-T calculations gave frequencies which were in quantitative disagreement with the Chu values. More seriously, the field pattern for the TM_{01} mode ($_eE_0$ in Chu's notation), was *qualitatively* different from that depicted in Chu's paper: URMEL-T yielded a field pattern that was basically a deformed version of the TM_{01} mode for the circular guide (a single, on-axis "flux tube" of E_z); Chu's solution showed a *pair* of E_z flux tubes, pointing in the *same direction*, located at what appeared to be the foci of the ellipse (see Fig. 1 below). Chu's picture also appeared to be at variance with the analytic form of the solution he presented for that mode.

A quick attempt to "arbitrate" the situation by using an approximate formula contained in McLachlan's classic work on Mathieu functions [2] yielded results which disagreed with both the above results. It was therefore decided that the most direct approach to resolving the various discrepancies, and to establishing URMEL-T's accuracy (at least for the ellipse problem) would be to solve the wave equation by numerical integration, using an iterative technique to obtain the relevant eigenvalues.

The original intent of this note was merely to summarize the results of the above investigation. However, it was felt that it would be useful to make the work reasonably self-contained, so that it could also serve a tutorial function, by including a discussion of the wave equation in elliptical coordinates and the properties of its solutions. We have also included two appendices, one on the elliptical coordinate system, and a second on a method for obtaining plots of transverse field lines. An abbreviated version of this note, restricted to a discussion of the analytical solutions and a comparison of Chu's results with those we obtained using numerical integration, has been submitted for publication[3].

2. The Wave Equation in Elliptical Coordinates

For a cylindrical waveguide (i.e. of constant cross-section), the z-dependence of the electric and magnetic fields is simply given by $e^{-jk_z z}$. Hence for TM (TE) waves, the wave equation for the longitudinal component of the electric (magnetic) field takes the form

$$\nabla_\perp^2 \begin{Bmatrix} E_z \\ H_z \end{Bmatrix} + (k^2 - k_z^2) \begin{Bmatrix} E_z \\ H_z \end{Bmatrix} = 0 \qquad (1)$$

* Work supported by the Director, Office of Energy Research, Office of High Energy and Nuclear Physics, High Energy Physics Division, U.S. D.O.E., under Contract No. DE-AC03-76SF00098.

where $\nabla_\perp^2$ represents the two-dimensional (i.e. in the transverse plane) Laplacian, and k is the wave number (ω/c) in unbounded space.

For a waveguide whose cross section is of the form of an ellipse of focal distance ρ, it is convenient to use confocal elliptical coordinates (see Appendix I). In this system, Eq. 1 can be rewritten as [4]

$$\frac{2}{\rho^2(\cosh 2\xi - \cos 2\eta)}\left(\frac{\partial^2}{\partial\xi^2}+\frac{\partial^2}{\partial\eta^2}\right)\begin{Bmatrix}E_z\\H_z\end{Bmatrix} + (k^2-k_z^2)\begin{Bmatrix}E_z\\H_z\end{Bmatrix} = 0 \tag{2}$$

Assuming that E_z (H_z) can be written in the form $U(\xi)\cdot V(\eta)$ [$\cdot e^{-jk_z z}$], we can rewrite Eq. 2 as

$$\frac{1}{U}\frac{\partial^2 U}{\partial\xi^2}+\frac{k^2-k_z^2}{2}\rho^2\cosh 2\xi = -\frac{1}{V}\frac{\partial^2 V}{\partial\eta^2}+\frac{k^2-k_z^2}{2}\rho^2\cos 2\eta \tag{3}$$

where by the usual argument, the left- and right-hand sides of Eq. 3 must be equal to a separation constant, which in accordance with conventional usage we define as a (not to be confused with the semi-major axis of the ellipse); a is actually the second spatial separation constant, the first one being k_z. We can then rewrite Eq. 3 as two separate equations

$$\frac{d^2U}{d\xi^2} - (a - 2q\cosh 2\xi)\,U = 0 \tag{4a}$$

$$\frac{d^2V}{d\eta^2} + (a - 2q\cos 2\eta)\,V = 0 \tag{4b}$$

where we have defined

$$q \equiv \frac{k^2-k_z^2}{4}\rho^2 \tag{5}$$

with q effectively replacing k_z as the first separation constant. Equation 4b for the "angular" dependence is the Mathieu equation; Eq. 4a, which gives the "radial" dependence, is usually known as the modified Mathieu equation.

Equations 4a and 4b exhibit some similarities with their polar-coordinate counterparts, but also significant differences. In both cases, solutions to the angular equation must exhibit a periodicity of 2π. However, in the polar coordinate case, only one of the separation constants appears in the angular equation. The periodicity requirement determines this constant; it can then be inserted into the radial equation, which can then be integrated numerically if necessary. For the elliptical equations, both constants appear in both equations, and so one must solve for both sets of eigenvalues simultaneously. If we denote the solutions of Eqs. 4a and 4b as $U(a,q;\xi)$ and $V(a,q;\eta)$, respectively, one chooses a given value of, say q, and then, by numerically integrating Eqs. 4a and 4b, finds the values of a which enable U and V to satisfy their respective boundary conditions, iterating until one can find a q for which both U and V require the same a.

We are now in a position to write down formally the solutions to Eq. 3. If we define

$$W(\xi,\eta) \equiv U(\xi)\cdot V(\eta)$$

then for TM modes (E waves), W describes the ξ,η-dependence of the E_z field; it must satisfy the boundary condition $U(\xi_o) = 0$, where ξ_o is the radial coordinate of the elliptical boundary. For TE modes (H-waves), W describes the H_z field, and satisfies the boundary condition $U'(\xi_o) = 0$.

In the usual fashion, one can obtain the transverse field components from the longitudinal field. Shown below are the relevant relations for elliptical coordinates; essentially these are the equations appearing in Refs. 1 and 2, albeit with slightly different notation. In all cases a z-dependence of $e^{-jk_z z}$ is understood; for completeness, we include the z-fields explicitly.

TE Modes:	TM Modes	
$H_z = A\,U(\xi)\,V(\eta)$	$E_z = A\,U(\xi)\,V(\eta)$	(6a,b)
$H_\xi = -\dfrac{E_\eta}{Z_{TE}} = -\dfrac{j\,k_z\,A\,U'(\xi)\,V(\eta)}{\rho_1\,(k^2-k_z^2)}$	$E_\xi = Z_{TM}H_\eta = -\dfrac{j\,k_z\,A\,U'(\xi)\,V(\eta)}{\rho_1\,(k^2-k_z^2)}$	(7a,b)
$H_\eta = \dfrac{E_\xi}{Z_{TE}} = -\dfrac{j\,k_z\,A\,U(\xi)\,V'(\eta)}{\rho_1\,(k^2-k_z^2)}$	$E_\eta = -Z_{TM}H_\xi = -\dfrac{j\,k_z\,A\,U(\xi)\,V'(\eta)}{\rho_1\,(k^2-k_z^2)}$	(8a,b)

where

$$Z_{TE} = \frac{\mu\omega}{k_z} = \frac{Z_o}{\sqrt{1-(\omega_c/\omega)^2}} \qquad Z_{TM} = \frac{k_z}{\varepsilon\omega} = Z_o\sqrt{1-(\omega_c/\omega)^2} \qquad (9a,b)$$

and

$$\rho_1 = \rho\sqrt{\cosh^2\xi - \cos^2\eta} = \rho\sqrt{\sinh^2\xi + \sin^2\eta} \qquad (10)$$

Finally, we note a point which will be of particular relevance in discussing the character of the solutions presented in Ref. 1. It might appear from the presence of the ρ_1 term in the denominators of Eqs. 7 and 8 that there is a singularity in the transverse fields at the points $\xi = 0$; $\eta = 0, \pi$, the foci of the ellipses; we will show now that this is not the case. In our discussion we will consider only the horizontal E-field at the right hand focus for the case of the TM modes; the arguments can easily be extended to all other cases.

For points on the x-axis to the right of $x = \rho$, $E_x = E_\xi$. Also, for these points $\eta = 0$, so that, from Eq. 7b we have

$$E_x(\xi,0) = -\frac{j\,k_z\,A\,U'(\xi)\,V(0)}{(k^2-k_z^2)\,\rho_1(\xi,0)} = C\,\frac{U'(\xi)\,V(0)}{\sinh\xi} \qquad (11a)$$

Similarly, for point on the interfocal line to the left of $x = \rho$, $E_x = -E_\eta$, and $\xi = 0$, so that from Eq. 8b we have

$$E_x(0,\eta) = -C\,\frac{U(0)\,V'(\eta)}{\sin\eta} \qquad (11b)$$

where the constant in Eq. 11b is the same as that in Eq. 11a. In the immediate neighborhood of $x = \rho$, we can approximate sinh ξ by ξ, sin η by η, $U'(\xi)$ by $U''(0)\,\xi = (a - 2q\cosh 2\xi)\,U(0)\,\xi$, and $V'(\eta)$ by $V''(0)\,\eta = (2q\cos 2\eta - a)\,V(0)\,\eta$ whereby we find that

$$\lim_{\xi\to 0} E_x(\xi,0) = \lim_{\eta\to 0} E_x(0,\eta) = (a - 2q)\,C\,U(0)\,V(0) \qquad (12)$$

From Eq. 12 we see that E_x is both finite and continuous at the point $(\xi,\eta) = (0,0)$.

It might appear that this result would admit of a sign change in E_x in the event that either $U(0)$ or $V(0)$ were zero at this point. However, as we shall see, the only way in which this can occur is for *both* solutions to be zero at that point, in which case the field is identically equal to zero along the entire length of the x axis.

2.1 Solutions to the Wave Equation and their Properties

By analogy with the circular functions, one can denote the $V(a,q;\eta)$ which satisfy the required periodic boundary conditions as $se_m(q;\eta)$ and $ce_m(q;\eta)$, depending on whether the function or its derivative is zero at $\eta = 0, 2\pi$. In fact, in the limit that $q\to 0$, $se_m(q;\eta)$ and $ce_m(q;\eta)$ approach sin mx and cos mx, respectively; moreover as with the circular functions, m is equal to the number of nodes in the interval $0 \le \eta < \pi$.[1] Note that in this notation, m has effectively replaced a as the second separation constant, with the various $V(a,q;\eta)$ of periodicity m defining a function $a_m(q)$ in the a-q plane; as may be seen from Eq. 4b, in the limit of $q = 0$, m is simply $\sqrt{a}$. The one other qualitative feature of the Mathieu functions worth noting at this point is their reflection symmetries about the points 0, $\pi/2$, and π, which are summarized in Table 1; note that for a continuous function, odd reflection symmetry about a point means the function has a value of zero at that point, and even reflection symmetry, a zero slope.

For the radial equation 4a, m has no special significance; however, since the constants in that equation must have the same values as those in the angular equation, it makes sense to label the radial solutions with m as well. By analogy with the hyperbolic trigonometric functions, one uses the notation $Se_m(q;\xi)$ and $Ce_m(q;\xi)$ for the two radial solutions. Note that the analogy applies only in distinguishing the solutions having zero value at the origin from those having zero slope; unlike the hyperbolic functions, the Se and Ce are oscillatory functions (for $q > 0$); in fact it is this oscillatory character that makes possible multiple radial eigensolutions (corresponding to different q) for a given m.

Table 1: Symmetries of the Mathieu functions under reflection about the angles 0, $\pi/2$, and π.

		REFLECTION ABOUT 0,π	
		Even	Odd
REFLECTION ABOUT $\pi/2$	Even	ce_{2n}	se_{2n+1}
	Odd	ce_{2n+1}	se_{2n+2} (se_{2n})

[1] Hence the lowest allowed m for the ce_m is 0 (as $q \to 0$, $ce_m(q;x) \to 1$), whereas for se_m it is 1.

Looking at the full solution, we note that there are two different kinds of $W(\xi,\eta)$, namely

$$W(\xi,\eta) = \mathrm{Ce}_m(q;\xi)\ \mathrm{ce}_m(q;\eta) \tag{13a}$$

$$W(\xi,\eta) = \mathrm{Se}_m(q;\xi)\ \mathrm{se}_m(q;\eta) \tag{13b}$$

sometimes referred to as even and odd solutions, respectively. Although it might seem initially that all combinations of the Ce, Se, ce, and se would be possible, continuity of both W and its vertical gradient across the interfocal line $\xi = 0$ restricts the allowed combinations to the two shown. This also substantiates our earlier assertion that solutions for which either $U(0)$ or $V(0) = 0$ require that the other be zero as well.

A requirement for the solutions of Eq. 4a to be non-divergent is that $q > 0$, a condition which Eq. 5 shows is always satisfied. A necessary requirement for the non-divergence of solutions to Eq. 4b is that $a > -|2q|$ [5]; for the case of $m = 0$, there is an additional constraint that $a < 0$. Since the ratio of V''/V at the points $\eta = 0,\pi$ has the value $2q - a$, for $m = 0$, those points represent local minima in the magnitude of V; for even $m > 0$, they will be local maxima for small q ($q < a/2 \approx m^2/2$), but local minima for larger q. These results will be seen to be relevant to the discussion of Chu's results.

2.2. Calculation of Eigenfrequencies

Of comparable importance to the field distributions are the frequencies of the various eigenmodes. The most direct method of calculating these frequencies is to use the doubly iterative numerical integration method described above, looking for combinations of a and q, which simultaneously satisfy the angular and radial boundary conditions. Having obtained the q (along with the a, or equivalently, the m) for a given mode, one can use Eq. 5 to obtain the mode frequency. Using the same convention as with circular geometry, we label the modes with the indices mr, with m, the index of the angular Mathieu function, indicating the number of oscillations between 0 and 2π, and r indicating that the radial solution corresponds to the rth root (i.e. value of q) of $U_m(q;\xi_o) = 0$ (for TM modes) or of $U_m'(q;\xi_o) = 0$ (for TE modes). In this notation,

$$f_{mr} = \frac{k_{mr}\, c}{2\,\pi} = \frac{c}{2\,\pi}\sqrt{\frac{4\,q_{mr}}{\rho^2} + k_z^2} \tag{14a}$$

For a cylindrical cavity of length ℓ, k_z is $n\pi/\ell$, where n is the number of longitudinal half-waves; for a wave guide, its value is unrestricted. In fact Eq. 14 can be used to find the cutoff frequency of the mr mode by setting $k_z = 0$, whereupon we have

$$f_{mr}^{cutoff} = \frac{c}{\pi\,\rho}\sqrt{q_{mr}} \tag{14b}$$

Chu's [1] method of arriving at the value of q_{mr} was somewhat similar. However, rather than numerically integrating the radial equation, Chu used Fourier-Bessel expansions of the Ce_m and Se_m, based on (at that time) unpublished M.I.T. tables. Starting with a given value of $k\rho$ (equivalent to assuming a q; see Eq. 5), he then calculated by successive approximation the value of ξ_o (or equivalently the eccentricity e–see Appendix I) for which the appropriate radial boundary conditions were satisfied, always restricting himself to the lowest radial root ($r = 1$); operationally this amounted to determining $e(q)$ rather than $q(e)$. In this way he could obtain a set of "universal" curves by plotting for each

mode the dimensionless quantity $k\rho$ as a function of e. Because of the specific problem he was considering, Chu instead chose the equivalent device of scaling the cutoff wavelength $\lambda_0 = 2\pi/k$ to the circumference of the ellipse. That quantity is given by

$$s = 4\rho/e \;\; \mathrm{E}(e) \tag{15}$$

where $\mathrm{E}(e)$ (sometimes written as $\mathrm{E}(\sin\alpha)$ or simply $\mathrm{E}(\alpha)$) is the complete elliptic integral of the second kind. It then follows that

$$\frac{\lambda_o}{s} = \frac{\pi e}{4\mathrm{E}(e)\sqrt{q}} = \frac{\pi e}{2\mathrm{E}(e)\, k\rho} \tag{16}$$

Having performed this procedure for the six lowest modes, Chu presumably interpolated on these curves (so as to get the appropriate q) to be able to calculate the fields for the case $e = 0.75$, the plots of which are presented in his paper.

A considerably more abridged means of arriving at q_{mr} is given by McLachlan, who presents the following approximate formulas for the roots of the Ce_m and Se_m; the results are parametrized in terms of e, rather than ξ_o.

Ce_{2m}:

$$q_{mr} = \{(r+1/2)\pi + (4m+1)\tan^{-1}[(1-e)/(1+e)]^{1/2}\}2e^2/4(1-e^2) \tag{17a}$$

For Ce_{2m+1}, the quantity $(4m+1)$ in Eq. 17a is replaced by $(4m+3)$.

Se_{2m+1}:

$$q_{mr} = \{(r+1)\pi + (4m+1)\tan^{-1}[(1-e)/(1+e)]^{1/2}\}2e^2/4(1-e^2) \tag{17b}$$

Similarly, for Se_{2m+2}, the quantity $(4m+1)$ in Eq. 17b is replaced by $(4m+3)$. McLachlan asserts that the accuracy of these formulas improves as both q and ξ (i.e., the order of the zero) increase; as we shall see, our own results support the latter assertion, but appear to contradict the former, at least for lowest order zeros.

The solutions to Eqs. 17a and 17b, when inserted in Eq. 14b, will yield the cutoff frequencies for the TM modes. To use these formulas for TE modes, one must rely on McLachlan's assertions that the "large zeros" of Ce'_m are in "close agreement" with those of Se_{m+1}, and those of Se'_m with those of Ce_{m-1}. We have not made a detailed study of the TE modes, and so cannot speak to the range of validity of these assertions; for the few cases in which we have applied it, the approximation appears of accuracy comparable to that of the determination of TM frequencies. However, note that as written, Eq. 17b will be in error by 1 in the denumeration of the radial order of all (even) TE modes for which $m > 0$: For "sufficiently large" q, $a - 2q < 0$, and so $\mathrm{Ce}''_m(0) > 0$, the first extremum of Ce_m will be the minimum following the first radial node, and the above correspondence of zeros is correct. However, for all $m > 0$, the lowest TE mode lies in the regime where $a - 2q > 0$, i.e. where $\mathrm{Ce}''_m(0) < 0$, so that the first zero of Ce'_m will be a maximum, and will be associated with a q for which there is no corresponding zero of $\mathrm{Se}_{m+1}(\xi_o)$. Two consequences follow from this: firstly, McLachlan's method cannot be used to predict the frequencies of the even TE_{m1} modes for $m \neq 0$; secondly, even though for the higher modes (i.e. the larger q) the rth zero of Ce'_m corresponds to the rth zero of Se_{m+1}, it corresponds to the $r+1$ (even) radial TE mode.

Table 2: Corresponding TE and TM modes in McLachlan's Approximation .

TE Modes		TM Modes	
Even $TE_{m,n}$	$\Rightarrow$	$m = 0$: Odd $TM_{m+1,n}$	
		$m > 0$: Odd $TM_{m+1,n-1}$	$(n > 1)$
		No counterpart	$(n = 1)$
Odd $TE_{m,n}$	$\Rightarrow$	Even $TM_{m-1,n}$	
Even $TE_{p-1,q}$ $(p = 1)$ Even $TE_{p-1,q+1}$ $(p > 1)$	$\Leftarrow$	Odd $TM_{p,q}$	
Odd $TE_{p+1,q}$	$\Leftarrow$	Even $TM_{p,q}$	

A summary of these correspondences, including the cases of the TE modes for which no counterpart modes exist, is summarized in Table 2. Recall that for the odd TE_{mn} (TM_{mn}) modes, the minimum allowed m is 1, whereas for the even ones, it is 0.

3. Comparison of Results

We compare the eigenmodes for two different ellipses as calculated using five different methods; these methods are:

1. Numerically integrating Eqs. 4a and 4b, and iterating until a common pair of a and q can be found which satisfy both the radial and angular boundary conditions.

2. The method used in Ref. 1, and summarized above; we do not repeat the calculations, but rather read from Figure 2 of that reference the q-values for the specified eccentricity for the lowest six modes of the elliptical waveguide.

3. Using the McLachlan formulas in Eqs. 17a and 17b to determine the q for which the appropriate boundary conditions are met.

4. Using the 2-dimensional field code URMEL-T to determine the cutoff frequencies of the various modes; in using this code, one specifies a frequency f^*, and the code returns the frequencies and fields of all modes having frequency $f < f^*$. To reduce the calculation time, we made use of the symmetries of the various field types and only solved for the fields in one quadrant of the ellipse, using boundary conditions (i.e., electric or magnetic wall) on the inter-quadrant boundaries to simulate the appropriate field symmetries. As will be discussed below, this had the additional salutory effect of reducing mode contamination.

5. Using the 2-dimensional field code URMEL. While URMEL results are much less sensitive to the choice of f^* than is URMEL-T, the code is limited in that it can only obtain solutions for TE modes.

The most detailed calculations were done on an ellipse of semi-axes of 6 and 2 cm , corresponding to an e of .94281; this is the geometry of the proposed ALS beam pipe.

Calculations using methods 1,2, and 3 were also done (for the lowest six modes) for an ellipse of semi-axes 10 and 6.614 cm, corresponding to an e of 0.75, the case for which the field plots are presented in Ref. 1.

Comparisons of the eigenfrequencies obtained using the various methods are presented in Tables 3 and 4. Since the Method 2 results were obtained by reading numbers off the curves in Ref. 1, they are only quoted to two decimal places. The McLachlan frequencies for the TE modes are shown in parentheses, since they are perforce equal to the corresponding TM frequencies; as noted above, this method does not give the frequencies for the lowest radial even TE modes for non-zero m. For the URMEL-T cases (Table 4), it was noticed that the accuracy of result for a given mode depended on how far its frequency lay below f^*; hence the URMEL-T results are tabulated showing the value(s) of f^* used in the calculation of a given mode's frequency.

Table 3: Eigenfrequencies for the six lowest modes of an ellipse of semi-major axis 10 cm and an eccentricity of 0.75 .

MODE	CUTOFF FREQUENCY (GHz)		
	Method 1 (*Num.Integ.*)	Method 2 (*Chu*)	Method 3 (*McLachlan*)
EVEN TE_{11}	.889	.88	—
ODD TE_{11}	1.300	1.30	(1.394)
EVEN TM_{01}	1.467	1.46	1.394
EVEN TM_{11}	2.124	2.11	1.915
EVEN TE_{01}	2.500	2.64	(2.527)
ODD TM_{11}	2.554	2.64	2.527

3.1 Chu's Results

Comparison of the first two columns in Tables 3 and 4 show that Chu's results (Method 2) are extremely accurate for the case of e =.75 (discrepancies here may simply be attributable to the accuracy with which one can read the values from the published curves). The reduced accuracy for the higher eccentricity, particularly the higher-frequency modes, is at least partly attributable to the fact that Chu is plotting the *wavelength*, rather than the frequency, and since the frequency for the higher modes increases with increasing eccentricity, a given reading error translates into a larger percentage error in the frequency; notwithstanding this consideration, the "exact" solutions (Method 1) clearly lie off Chu's curves for the higher eccentricity. This would suggest that the accuracy of either the tables or the truncated expansions used by Chu decreases in the limit of large q and small ξ.

Perhaps more striking than the agreement in frequency for the modes of the $e = 0.75$ ellipse is the fact that the figure presented for the fields of the even TM_{01} (or $_eE_o$) mode, shown in Fig. 1, reproduced from Ref. 1, are *qualitatively incorrect* (this *despite* the fact that the cutoff frequency for this mode is correctly calculated in Ref. 1!). This can be seen in several ways.

Table 4: Comparative calculation of eigenfrequencies of an ellipse of semi-major axis 6 cm and semi-minor axis of 2 cm ($e \approx 0.94$) .

MODE	CUTOFF FREQUENCY (GHz)					
	Method 1 (*Num.Integ.*)	Method 2 (*Chu*)	Method 3 (*McLachlan*)	Method 4 (*URMEL-T*) *Best f*	*f**	Method 5 (URMEL)
EVEN TE_{11}	1.496	1.457		1.489	1.508	1.4953
ODD TE_{11}	4.095	4.31	(4.15)[b]	4.116	5.5	4.0864
EVEN TM_{01}	4.205	4.49	4.15	4.246[a]	4.55	
EVEN TM_{11}	5.11	5.91	4.96	5.138	5.5	
EVEN TM_{21}	6.08		5.77	6.109	6.15	
EVEN TE_{01}	7.876	12.5	(7.90)[b]	7.98	15.	7.8541
ODD TM_{11}	7.92	12.5	7.90	8.032	11	
EVEN TM_{41}	8.17		7.40	8.175	8.193	
ODD TM_{21}	8.78		8.71	8.833	9.2	
EVEN TE_{22}	9.60		(9.52)[b]	9.627	11	9.5903
EVEN TM_{61}	10.38		9.02	10.363	11	
EVEN TM_{02}	11.66		11.66	11.92[c]	15	
EVEN TM_{12}	12.50		12.46	12.74[c]	15	
EVEN TM_{22}	13.36		13.27	13.35/71[c]	25	
EVEN TM_{62}		17.05	16.46	17.20/66[c]	25	

[a] Using an f^* of 5.1 GHz, the frequency of this mode was calculated to be 4.257 GHz.
[b] Cutoff frequencies for TE modes, as estimated using method 3, are perforce degenerate with those for corresponding TM modes (see text).
[c] Reduced type sizes indicate uncertainty in mode identification (see text).

Figure 1 shows a reversal in the sign of E_x as x increases. However, Eqs. 11a and 11b show that the relative signs of E_x on either side of the focus[2] depend on the relative signs of $Ce_0'(\xi)$ and $ce_0'(\eta)$. We have plotted these functions in Figs. 2 and 3, respectively, for the case of an ellipse with $e = 0.75$ and with a q corresponding to the cutoff frequency of its TM_{01} mode. From Fig. 2, we see that the sign of $Ce_0'(\xi)$ is everywhere negative; from Fig. 3, that the sign of $ce_0'(\eta)$ is positive throughout the region $0 \le \eta \le \pi/2$. (In fact, both these results are true for *any* positive value of q, provided the radial function has its first zero at the outer boundary.) Hence, from Eqs. 11a and 11b, we see that the sign of E_x is the same for all positive x, in direct contradiction to the figure.

[2]We have already shown, in the discussion accompanying Eq. 12, that E_x is both finite and continuous *at* the focus.

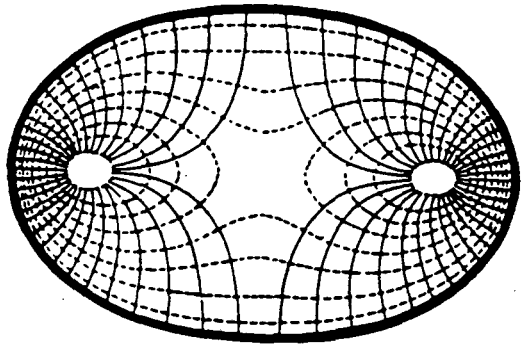

Figure 1. Field pattern for the TM_{01} mode for an ellipse of $e = 0.75$, as shown in Ref. 1. Both the initial increase in E_z and the change of sign of E_z with increasing x are inconsistent with the analytic expression for the field (see text).

Since the transverse fields are derivable from the longitudinal fields, we might also expect a contradiction to arise with respect to E_z, and this is in fact the case. Figure 1 suggests that the value of E_z on the x-axis initially increases with x, reaching a maximum at a point which appears to be the focus of the ellipse (although the point is not explicitly identified as such in Ref. 1); in elliptical coordinates this would correspond to η decreasing from $\pi/2$ to 0 (see Fig. A.I.1 in Appendix I). However, as shown in Fig. 3, ce_0 is a *maximum* at $\eta = \pi/2$, meaning that E_z decreases with increasing x. In fact, similar to the result for the transverse field, this angular dependence of E_z characterizes not only this particular TM_{01} mode, but rather *any* $m = 0$ mode (for *any* positive q, and hence any eccentricity).

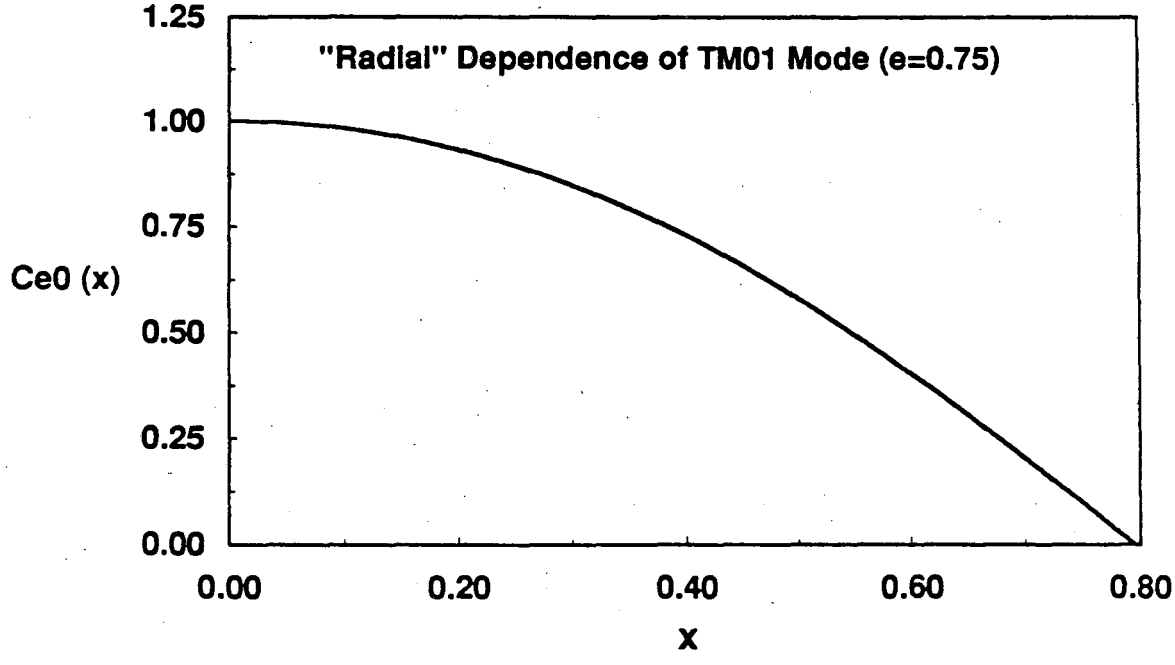

Figure 2. Radial dependence of E_z for the TM_{01} mode for an ellipse with $e = 0.75$, i.e. a plot of $Ce_{01}(q;x)$ for the q corresponding to the aforementioned mode.

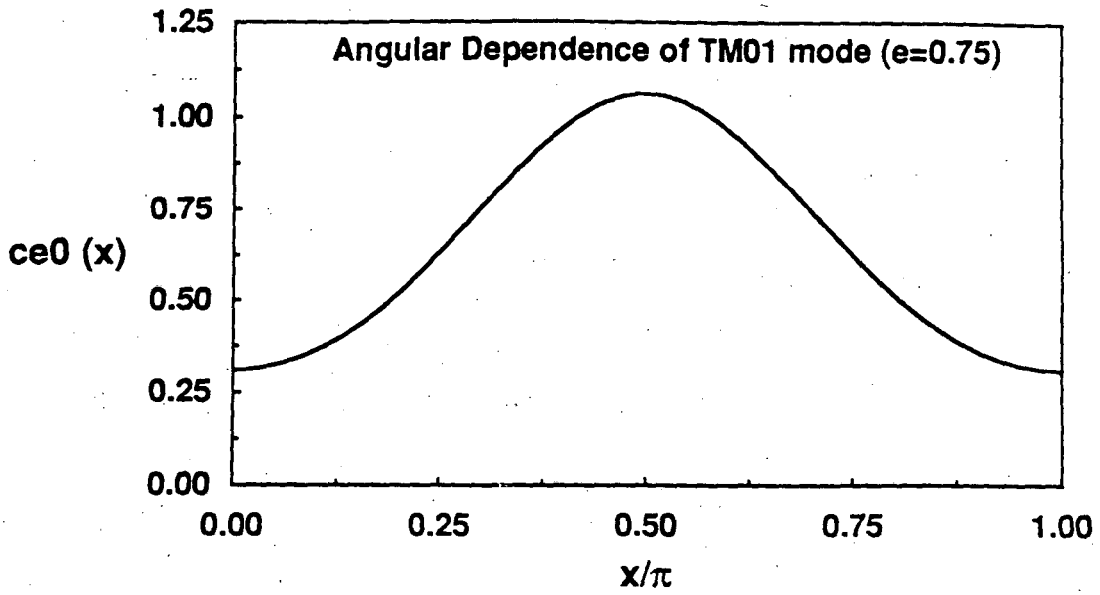

Figure 3. Angular dependence of E_z for the TM_{01} mode for an ellipse with $e = 0.75$, i.e. a plot of $ce_1(q;x)$ for the q corresponding to the aforementioned mode.

The true appearance of the electric field for the TM_{01} mode is as shown in Fig. 4,[3] essentially a deformed version of the corresponding mode for a circular guide, a result which holds for all values of q and e. This result, although not particularly surprising, is by no means a universal occurrence. In particular, as far as bifurcation of flux tubes is concerned, this can indeed occur in the transition between circular and elliptic geometries, although it generally happens in the *reverse* sense: For example, for the even TM_{m1} modes with $m > 1$, what are single flux tubes in moderately eccentric elliptical geometry can bifurcate as the geometry becomes more nearly circular.

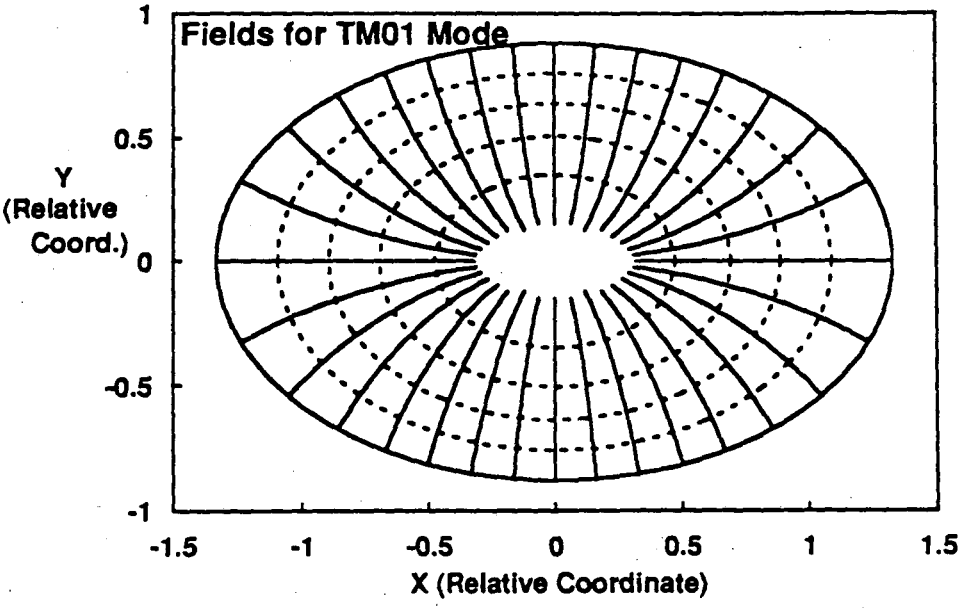

Figure 4. Field pattern for the TM_{01} mode for an ellipse of $e = 0.75$, obtained from the numerically integrated solutions as described in the text; the field-line conventions are the same as in Fig. 1.

[3]The procedures for obtaining such plots are described in Appendix II.

It is perhaps a fruitless endeavor to speculate on the origin of the erroneous field plot in Ref. 1; however, one cannot help but conjecture. The most likely (and, in our view, the only plausible) explanation is that when the fields were calculated, the values of $ce_0(q;\eta)$ used to generate the fields were, for one reason or other, those corresponding to a *negative* q, albeit with the correct magnitude (the values of $Ce_0(q;\xi)$ would still have had to be calulated correctly). This would have interchanged the nature of the extrema at $\eta = 0$ and $\pi/2$ and reversed the relative field directions on either side of the foci, consistent with the field plots in Ref. 1.

3.2 The McLachlan Method

From Tables 3 and 4 we see that McLachlan's formula (Method 3) consistently predicts too low a frequency for the TM_{mn} modes. The discrepancy is seen to increase with increasing m, but decrease with increasing n; in the relatively few cases examined, it was greater for the even modes than the corresponding odd ones. Interestingly, while the frequencies the method predicts for those TE modes for which it applies are perforce degenerate with those of corresponding TM modes (in this case "corresponding" implies *different* mode numbers; see the last paragraph in Sect. 4), in all cases looked at, the TE modes had lower frequencies than their TM counterparts, and the McLachlan estimates turned out to lie at a value intermediate to the two, with comparable percentage discrepancy. In contrast with Chu's method, for the two ellipses examined, the accuracy of McLachlan's method appears to increase with increasing eccentricity. In general, the results for $n > 1$ appear accurate to a few percent, and for the $n = 1$ modes, the method appears to provide a reasonable initial guess for solutions to be obtained by Method 1.

3.3 URMEL-T Results

The URMEL-T results (Method 4) are shown in Table 4. As alluded to above, the closer f^* is to the cut-off frequency of a given mode (i.e., the lower it is), the more accurately it determines that frequency. The likely cause for this appears to be that URMEL-T (unlike its predecessor code URMEL) does not solve directly for the cutoff frequency (or more precisely the cutoff wave number, k_c) but rather for the propagation constant k_z at frequency f^*. It then obtains k_c by taking

$$k_c = \sqrt{k^{*2} - k_z^2} \tag{18}$$

If $f^* >> f_c$, this results in a differencing of large numbers. Assuming the error in determining k_c is more or less constant, the resulting percentage error in determining k_c will be larger for large f^*.

For the lowest radial mode corresponding to a given m, even for the larger values of f^*, URMEL-T gives results which are more accurate than those of the McLachlan method; for the higher radial modes, the McLachlan approximation appears to give the more accurate result. The frequencies URMEL-T finds are consistently higher than the actual frequencies. The latter effect might be thought to be the result of approximating the ellipse by a polygon, since for any non-reentrant curved figure, such a polygon has an area less than that of the figure, and so might be expected to have a slightly higher frequency. However, when we used URMEL-T to find the eigenmodes of a rectangular cavity, it consistently found frequencies *lower* than the predicted values.

At the higher frequencies, the mode density increases, and identification of given modes is less certain. To facilitate identification, we looked at the associated field plots. However, at these frequencies, the character of the modes was not always clear, and in some instances there appeared to be contamination by other modes of nearby frequency having the same field symmetry (including mixing of TM and TE modes). In this regard, the "quartering" of the ellipse and the use of inter-quadrant boundary conditions served to reduce the instances of such mode contamination, but not eliminate them altogether. The frequencies obtained for modes which could not be unambiguously identified are shown in reduced typeface in Table 4.

3.4 URMEL Results

Of all the other methods looked at, Urmel consistently yields values which are closest (generally within better than 0.5%, mostly better than 0.1%) to those obtained by numerical integration. However, despite the fact that it employs a rectangular grid, and thereby underestimates the cross sectional area, it appears consistently to calculate too *low* a cutoff frequency (see the previous comments on URMEL-T). Also, because it calculates k_c directly (see above discussion on URMEL-T), URMEL also proves to be much less sensitive than URMEL-T to the value of f^*. It also has the nice feature, possibly made possible because it employs a rectangular grid, of providing plots of the transverse field lines (see the comments in Appendix II). Unfortunately, it can only calculate TE fields, and is therefore of limited interest for beam dynamics studies.

4. Conclusions

Both URMEL-T and the McLachlan approximation appear to give reasonable values for the cutoff frequencies of elliptical waveguides; both are less accurate than URMEL, which unfortunately suffers from the drawback that it can only solve for TE modes The accuracy of the McLachlan method appears to be greater for higher-order radial modes, lower-order angular modes, and increased eccentricity. On the other hand, URMEL-T gives results which, while not always as accurate as McLachlan's, appear to be more uniformly accurate over a variety of modes. URMEL-T's drawbacks are the necessity for adjusting the search frequency f^* depending on the frequencies of the modes being searched for, and the mixing of nearby modes having the same boundary conditions. As noted, this problem can be ameliorated by subdividing the ellipse along its symmetry planes, thereby eliminating any contaminant modes which fail to satisfy the same boundary conditions on the symmetry planes. It may also be possible use URMEL as a means of increasing the confidence in the URMEL-T results, by checking the latter's calculation of TE mode frequencies, and also helping to identify which of the ambiguous modes is either a TE mode, or suffers from TE contamination.

The original dilemma which led to this detailed a study of the problem has been resolved. The value which Chu obtained for the TM_{01} was correct; the field plot for that mode was not. The discrepancy between the Chu and McLachlan results was simply due to the inaccuracy of the latter; that between the Chu and URMEL results, the result of starting the latter calculation with too large a value for f^*.

Finally, there is the question of the general usefulness of URMEL-T, and the confidence one can have in its results for cavities of other shapes, where "exact" solutions do not exist. For lower frequencies, where the mode density is low, for a given f^* one can expect modes of $f \geq f^*/2$ to be accurate to a few percent. For the higher-frequency

modes, confidence can be increased by using the above subdividing technique, multiple choices of f^*, and examination of field plots, as well as conjoint use of URMEL, to try to identify and/or eliminate instances of mode contamination. Also, as we intend to show in an accompanying note, for reasonably regular shapes, one can usually determine a systematic progression of modes, based on the progression one observes in (and using the nomenclature associated with) simpler geometric structures, such as the ellipse or the rectangle; establishing such a mode progression helps in identifying potential missing modes and contaminated ones, as well as identifying gross abnormalities which may occur in the mode frequencies.

Acknowledgements

This work was largely stimulated by G.R. Lambertson's suggestion that the solution for the TM_{01} mode pictured in Ref. 1 seemed to be incorrect. Discussions of this problem with both G.R. Lambertson and D. L. Judd have been both stimulating and informative. The code to calculate the the frequencies predicted by the McLachlan formula was written by Y.-H. Chin.

References

1. Chu, Lan-Jen, "Electromagnetic Waves in Elliptic Hollow Pipes of Metal," J. Appl. Phys. **9**, 583 (1938); much of Chu's article has been reproduced in Marcuvitz, N., *Waveguide Handbook*, (Peter Peregrinius, London, 1986), pp. 80-84.
2. McLachlan, N.W., *Theory and Application of Mathieu Functions,* (Clarendon, Oxford, 1947), pp. 241-242.
3. Goldberg, D.A., Laslett, L.J., and Rimmer,. R.A. "Modes of Elliptical Waveguides: A Correction", to be published.
4. Blanch, G., in *Handbook of Mathematical Functions*, edited by M. Abramowitz and I.A. Stegun (Dover, New York, 1972), p. 722
5. See Ref. 2; p.236.
6. V. Brady, "Three-Dimensional Field Components," LBL HIFAR Note 261 (unpublished).
7. V. Brady, "Three-Dimensional Field Tests," LBL HIFAR Note 262 (unpublished).

APPENDIX I: ELLIPTICAL CO-ORDINATES

The polar coordinate system is constructed using as the radial coordinate a set of *concentric* circles (each characterized by a size coordinate, the radius), with the orthogonal coordinate being a set of lines through the same center as the circles. In like manner one can construct an elliptical coordinate system using as the "radial" coordinate a set of *confocal* ellipses, with the orthogonal coordinate being a set of hyperbolas having the same foci (see Figure A.I.1). The following discussion provides a "derivation" of the elliptical coordinate system, as well as a summary of the principal formulas associated with ellipses and elliptical coordinates.

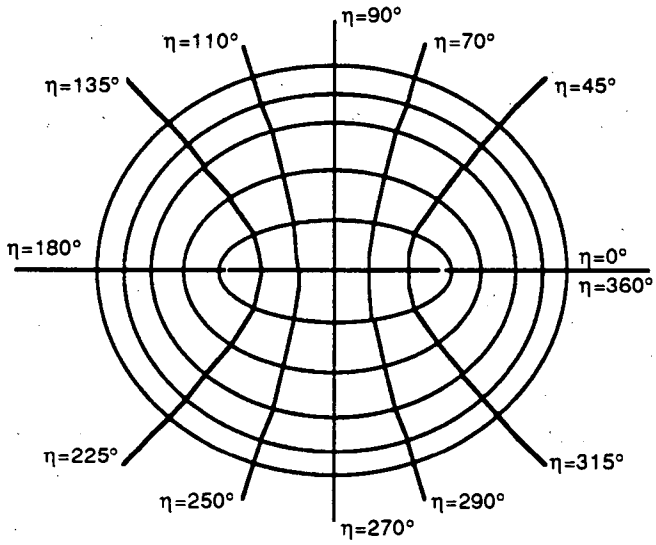

Fig. A.I.1

The semi-major and semi-minor axes of an ellipse, a,b, are related to the focal distance ρ by

$$\rho = \sqrt{a^2 - b^2} \qquad \text{(A.I.1)}$$

If we formally define the quantity ξ by the relation $\xi \equiv \cosh^{-1}(a/\rho)$, then Eq. A.I.1 will be satisfied, provided that $b = \rho \sinh \xi$, i.e.

$$a = \rho \cosh \xi \qquad\qquad b = \rho \sinh \xi \qquad \text{(A.I.2a,b)}$$

Moreover, if we now introduce the variable η and formally define

$$x = \rho \cosh \xi \cos \eta \qquad\qquad y = \rho \sinh \xi \sin \eta \qquad \text{(A.I.3a,b)}$$

we see that the x and y so defined satisfy the ellipse equation

$$\frac{x^2}{a^2} + \frac{y^2}{b^2} = 1 \qquad \text{(A.I.4)}$$

and so Eqs. 3a and 3b serve to connect the ellipse-related coordinates (ξ,η) to the familiar

cartesian coordinates.

In addition to the quantities a, b, ρ which can characterize an ellipse, we can add a fourth quantity, the eccentricity e, defined by

$$e = \rho/a \tag{A.I.5}$$

The limiting cases are: $e = 0$, which describes a circle; $e = 1$, which, from Eq. A.I.1 implies $b/a \rightarrow 0$, and can describe either a straight line of length 2ρ ($b \rightarrow 0$) or a parabola (the location of one of the foci remains finite; the other focus, the center of the ellipse, and b all $\rightarrow \infty$, but b/a still $\rightarrow 0$). Note that ξ is related to e by

$$\xi = \cosh^{-1}(1/e) \tag{A.I.6a}$$

from which it follows that b can be related to e by

$$b = \frac{\rho}{e}\sqrt{1-e^2} \tag{A.I.6b}$$

Normally one needs *two* of the above quantities to specify a given ellipse, e.g. the semi-major and semi-minor axes. However, if one creates a coordinate system which uses a set of *confocal* ellipses[4] (thereby specifying ρ) only a single additional parameter is needed, i.e. with ρ specified, the various ellipses in Fig. A.I.1 can be identified any *one* of the other parameters listed above. It will probably come as no surprise that the parameter one chooses is ξ; among the reasons that this proves to be a convenient choice is that the smallest of the confocal ellipses, the straight line running from $-\rho$ to $+\rho$, is characterized by $\xi = 0$.

It will probably also come as no surprise that the choice of the second coordinate turns out to be η. If we define the quantities α,β by

$$\alpha = \rho \cos \eta \qquad\qquad \beta = \rho \sin \eta \tag{A.I.7a,b}$$

then coordinate pairs (x,y) corresponding to a given η satisfy the equation

$$\frac{x^2}{\alpha^2} - \frac{y^2}{\beta^2} = 1 \tag{A.I.8}$$

i.e., they describe a set of hyperbolae which one can straightforwardly show are confocal with and orthogonal to the confocal ellipses, as shown in Fig. A.I.1.

From Eqs. A.I.3a,b we can obtain the expression for the metric coefficients or scale factors

$$h_\xi = h_\eta = \rho\sqrt{\tfrac{1}{2}(\cosh^2\xi - \cos^2\eta)} = \rho\sqrt{\tfrac{1}{2}(\sinh^2\xi + \sin^2\eta)} \tag{A.I.9}$$

from which we can obtain the differential path length in elliptical coordinates

$$ds = \rho\sqrt{(\cosh^2\xi - \cos^2\eta)\,(d\xi^2 + d\eta^2)} \tag{A.I.10}$$

[4]Since one almost invariably uses elliptical coordinates to solve a problem involving an elliptical boundary, one uses as "radial" coordinates those ellipses which are confocal with the boundary ellipse.

One also has the following inverse relations. If the points (x,y) lie on an ellipse of focal length ρ, then the semi-major axis of the ellipse ζ is defined by

$$2\zeta^2 = x^2 + y^2 + \rho^2 \sqrt{(x^2 + y^2 + \rho^2)^2 - 4\rho^2 x^2} \qquad \text{(A.I.11)}$$

from which one can obtain

$$\xi = \cosh^{-1}(\zeta/\rho) \qquad \eta = \cos^{-1}(x/\zeta) \qquad \text{(A.I.12)}$$

Finally, if one obtains the solutions to the field equations in elliptical coordinates, he generally needs to convert the (ξ,η) field components to (x,y) components (say for plotting purposes). Since the (ξ,η) system provides a pair of locally orthogonal coordinates, the usual transformation equations apply, viz:

$$E_x(x,y) = E_\xi\,(x,y)\cos\vartheta_{\xi x} - E_\eta(x,y)\sin\vartheta_{\xi x} \qquad \text{(A.I.13a)}$$

$$E_y(x,y) = E_\xi\,(x,y)\sin\vartheta_{\xi x} + E_\eta(x,y)\cos\vartheta_{\xi x} \qquad \text{(A.I.13b)}$$

where the values of x and y are obtained from the (ξ,η) at which the fields were actually calculated using Eqs. A.I.3a and A.I.3b, and $\vartheta_{\xi x}$, the angle between the ξ- and x-directions, is given by

$$\tan\vartheta_{\xi x} = \left.\frac{dy}{dx}\right|_\eta = \frac{\tan\eta}{\tanh\xi} \qquad \text{(A.I.14)}$$

from which it follows that

$$\cos\vartheta_{\xi x} = \frac{\tanh\xi}{\sqrt{\tanh^2\xi + \tan^2\eta}} \qquad \sin\vartheta_{\xi x} = \frac{\tan\eta}{\sqrt{\tanh^2\xi + \tan^2\eta}} \qquad \text{(A.I.15a,b)}$$

where consistent signs can be obtained by using the negative value of the radical in the second and third quadrants.

APPENDIX II: A METHOD FOR OBTAINING FIELD LINES FOR THE TRANSVERSE COMPONENTS OF ELECTRIC AND MAGNETIC FIELDS

We describe here a procedure which can be used to obtain field lines for the transverse components of E and H fields. We will discuss specifically the case of TM modes; the generalization to the case of TE modes is obvious. It is assumed in the ensuing discussion that the longitudinal and transverse components of the fields (the latter may be in non-cartesian coordinates) have already been evaluated. As will be seen, the procedure is most readily applied to cases, such as the present problem, in which the boundary conditions permit a separation of variables; however, with some additional effort, it can also be applied to field solutions obttained from numerical field solvers.

For a TM mode, E_z is proportional to the vector potential for the (transverse) H field. Hence, lines of constant E_z are field lines of H, and uniform spacing of contours of constant E_z results in a line density proportional to the value of the local H field. With a numerical field solver such as URMEL, E_z would be directly available as output; for the present problem E_z can be readily obtained by taking the (previously obtained) numerical solutions to Eqs. 4a and 4b, and substituting them into Eq. 6b. For the present problem, finding field contours is quite straightforward; for fields obtained from a numerical field solver, the problem may be somewhat more complicated, depending on the density and regularity of spacing of field points.

Obtaining the E fields is somewhat more difficult; moreover the degree of difficulty depends on whether the solutions have been obtained by separation of variables and numerical integration or by a numerical field solver such as URMEL, and, if the latter, whether the solver employs a regular or irregular (e.g. triangular) mesh. We will treat the specific example of an elliptical geometry; the results are readily generalized to any planar coordinate system.

In any planar coordinate system, the E-field lines are characterized by the relation

$$\frac{dx_2}{dx_1} = \frac{h_1}{h_2}\,\frac{E_{x_2}}{E_{x_1}} \qquad \text{(A.II.1a)}$$

where x_1 and x_2 are the two (orthogonal) transverse coordinates and h_1 and h_2 are the metric coefficients, or scale factors; in the present problem, the coordinates are ξ and η, respectively. From Eq. A.I.9, we see that Eq. A.II.1a then takes the form

$$\frac{d\eta}{d\xi} = \frac{E_\eta}{E_\xi} \qquad \text{(A.II.1b)}$$

Differential equations of the general form

$$\frac{d\eta}{d\xi} = f\,[u_1(\xi,\eta), \ldots, u_n(\xi,\eta),\ \eta;\ \xi\,] \qquad \text{(A.II.2)}$$

(i.e., such as Eq. A.II.1) can be solved using a numerical integration technique such as the Runge-Kutta (R-K) method. In using this method, one successively calculates the $\eta_{m+1}(\xi_{m+1})$ by integrating from $\eta_m(\xi_m)$ with the initial condition $\eta'_m(\xi_m) = f_m$.

In general, the field point (ξ_{m+1}, η_{m+1}) which results from the mth integration step is not a point for which the original field solutions were obtained; hence, it would appear that at each step an interpolation of those fields would be necessary in order to obtain a starting value of f_{m+1} to use for the next integration step. If this is indeed the case, then clearly such an interpolation will be simpler if the original field mesh is rectangular (as it is for URMEL) than if it is both irregular and triangular (as it is for URMEL-T).[5] However, if the problem is amenable to a separation of variables, the task can be considerably simplified.

First, we note that one can apply the R-K method to a *set* of coupled differential equations of the form

$$\frac{du_i}{d\xi} = f_i\,[u_1(\xi,\eta), \ldots, u_n(\xi,\eta);\ \xi\,] \tag{A.II.3}$$

where the absence of η as a separate dependent variable on the the right hand side simply reflects the fact that we formally consider it as one of the u_i (for simplicity, we will consider it to be u_1). In the present problem, for example, from Eqs. 7b and 8b, we have

$$\frac{E_\eta}{E_\xi} = \frac{U(\xi)\,V'(\eta)}{U'(\xi)\,V(\eta)} \tag{A.II.4}$$

Combining with Eq. A.II.1b gives for the first of Eqs. A.II.3

$$\frac{d\eta}{d\xi} = \frac{U(\xi)\,V'(\eta)}{U'(\xi)\,V(\eta)} \tag{A.II.3.1}$$

If we define U and U' to be u_2 and u_3, respectively, then the second and third of Eqs. A.II.3 become

$$dU/d\xi = U' \tag{A.II.3.2}$$

and

$$dU'/d\xi = \partial^2 U/\partial\xi^2 = (a - 2q\cos 2\xi)U \tag{A.II.3.3}$$

To obtain the two remaining equations (for u_4 and u_5 equal to V and V'), we note that since we are looking for the derivative with respect to ξ *along the integration path* (i.e. the field line), the respective derivatives for V and V' are $dV/d\xi = \partial V/\partial\eta \cdot d\eta/d\,\xi$ and $dV'/d\xi = \partial^2 V/\partial\eta^2 \cdot d\eta/d\,\xi$, where for $d\eta/d\,\xi$ we simply use the expression in A.II.3.1. The remaining two equations are then

$$dV/d\xi = V'\,d\eta/d\,\xi \tag{A.II.3.4}$$

and

$$dV'/d\xi = (-a + 2q\cos 2\eta)\,V\,d\eta/d\,\xi \tag{A.II.3.5}$$

It is the separability of variables that makes possible the replacement of the second derivatives in Eqs. A.II.3.3 and A.II.3.5 by the functions (and possibly, in the more general case, their first derivatives), and hence a set of equations of the form given in A.II.3. The great benefit in having a set of equations of this form is that the results of the

[5]Two recent LBL technical reports [6,7] describe how such an interpolation can be performed on such a triangular mesh for solutions of Laplace's equation in the r-z plane.

integration at step m yield not only the path coordinate $\eta_{m+1}(\xi_{m+1})$, but also the values of U, V, U', and V' at that point, which are needed for integrating the $m+1$st step (thereby precluding the need for interpolation). Note that for the *first* step, we can begin integrating at the outer boundary, and so can choose as our starting point a (ξ, η) pair from the original numerical solutions of Eqs. 4a and 4b, i.e. one for which we know the initial values for U, U', V, and V'. (This would be the procedure even in the cases where separation of variables was *not* possible.)

We would like to choose a set of starting coordinates for the R-K method that produce a line density proportional to the field strength, as was done with the H-field lines. In general, this would mean numerically integrating $\mathbf{E}_{\perp} ds$ (using the previously obtained field values) along the outer boundary, and choosing as starting points for the R-K method, coordinates which produced equal increments in the flux integral. In general this integral will be simpler to calculate in the case of separable variables (where the path is defined by a single coordinate). For an elliptical boundary, we have from Eqs. 7b and A.I.10 (see Appendix I) that the flux of the electric field on the outer boundary takes the particularly simple form

$$\int E_{\xi}\, ds \propto \int V(\eta)\, d\eta \qquad \text{(A.II.5)}$$

where we use the previously obtained solutions to Eq. 4b as the values for the integrand.

LAWRENCE BERKELEY LABORATORY
UNIVERSITY OF CALIFORNIA
INFORMATION RESOURCES DEPARTMENT
1 CYCLOTRON ROAD
BERKELEY, CALIFORNIA 94720